



Cite this: *Dalton Trans.*, 2016, **45**, 15994

Changing the chemical and physical properties of high valent heterobimetallic bis-(μ -oxido) Cu–Ni complexes by ligand effects[†]

Maria-Chrysanthi Kafentzi,^a Maylis Orio,^a Marius Réglier,^a Shenglai Yao,^b Uwe Kuhlmann,^b Peter Hildebrandt,^b Matthias Driess,^{*b} A. Jalila Simaan^{*a} and Kallol Ray^{*c}

Two new heterobimetallic $[\text{LNiO}_2\text{Cu}(\text{RPY2})]^+$ (RPY2 = *N*-substituted bis 2-pyridyl(ethylamine) ligands with R = indane, **3a** or R = Me, **3b**) complexes have been spectroscopically trapped at low temperatures. They were prepared by reacting the mononuclear *side-on* LNi^{II} superoxo precursor bearing a β -diketiminate ligand ($\text{L} = [\text{HC}-(\text{CMeNC}_6\text{H}_3(\text{iPr})_2)_2]$) with the Cu(i) complexes. In contrast to the oxo groups in known high-valent $[\text{M}_2(\mu\text{-O})_2]^{n+}$ ($\text{M} = \text{Fe, Co, Ni, Cu}$) cores that display electrophilic reactivities, **3a** and **3b** display rather nucleophilic oxo cores active in aldehyde deformylation reactions. However, the spectroscopic and reactivity properties of **3a**/**3b** are found to be distinct relative to that of the previously reported $[\text{LNiO}_2\text{Cu}(\text{MeAN})]^+$ complex containing a more basic (nucleophilic) *N,N,N',N'*-pentamethyl-dipropylenetriamine (MeAN) ligand at the copper centre. The geometry and electronic properties of the copper ligands affect the electron density of the oxygen atoms of the heterodinuclear $\{\text{Ni}(\mu\text{-O})_2\}$ core and **3a**/**3b** undergo slower nucleophilic and faster electrophilic reactions than the previously reported $[\text{LNiO}_2\text{Cu}(\text{MeAN})]^+$ intermediate. The present study therefore demonstrates the tuning of the electrophilicity/nucleophilicity of the oxygen atoms of the heterobimetallic $[\text{Ni}(\mu\text{-O})_2\text{Cu}]^{2+}$ cores by controlling the electron donation from the ancillary ligands, and underlines the significance of subtle electronic changes in the physical and chemical properties of the biologically relevant heterobimetallic metal–dioxygen intermediates.

Received 15th June 2016,
Accepted 28th July 2016
DOI: 10.1039/c6dt02391f
www.rsc.org/dalton

Introduction

The synthesis and characterisation of metal–oxygen intermediates are very important for understanding the mechanisms of transition metal mediated dioxygen activation reactions taking place in chemical and biological systems. In this context homobimetallic bis(μ -oxido) complexes with $[\text{M}_2(\mu\text{-O})_2]^{n+}$ cores have attracted much attention and they have been extensively studied for systems involving Cu,¹ Mn,² Ni,³ Co,⁴ Fe,⁵ and Pt centres.⁶ In particular, homobimetallic copper dioxygen cores have been the subject of extensive investigations due to their possible involvement in biological oxidation reactions as key intermediates in phenol hydroxylation by tyrosinase,⁷ as well

as in methane oxidation by particulate methane monooxygenase.⁸

In contrast to the homobimetallic systems, the properties of mixed-metal dioxygen species have been less explored. These types of intermediates are probably involved in various catalytic processes in metalloenzymes; for example, in cytochrome c oxidase, where a Cu^I ion cooperates with an Fe^{II}(heme) to activate dioxygen or in Cu–Zn superoxide dismutase, in which the superoxido ligand disproportionation is mediated through a mixed Cu–Zn metal site. The generation and the study of such mixed metal species are therefore of significant interest due to the unique properties obtained by the combination of two different metal ions. The synthesis of heterodinuclear complexes, however, presents a special challenge because of the possibility of disproportionation and selectivity problems resulting in the formation of mixtures of homo- and heterodinuclear complexes, as well as metal-site isomers. In order to overcome these problems two main strategies were previously used in the literature (Fig. 1).⁹

The first one involves the synthesis of ligands providing different coordination environments that are specific for each of the two metal ions. An alternative route is the reaction of a

^aAix Marseille Univ, CNRS, Centrale Marseille, iSm2, Marseille, France.

E-mail: jalila.simaan@univ-amu.fr

^bDepartment of Chemistry, Technische Universität Berlin, Straße des 17. Juni 135, 10623 Berlin, Germany. E-mail: matthias.driess@tu-berlin.de

^cDepartment of Chemistry, Humboldt-Universität zu Berlin, Brook-Taylor-Straße 2, 12489 Berlin, Germany. E-mail: kallol.ray@chemie.hu-berlin.de

[†]Electronic supplementary information (ESI) available. See DOI: [10.1039/c6dt02391f](https://doi.org/10.1039/c6dt02391f)



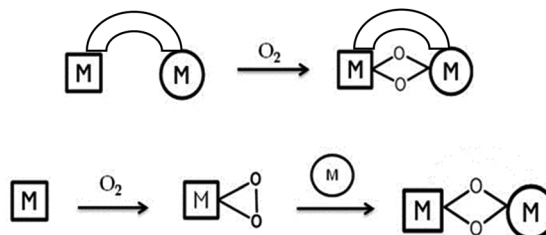
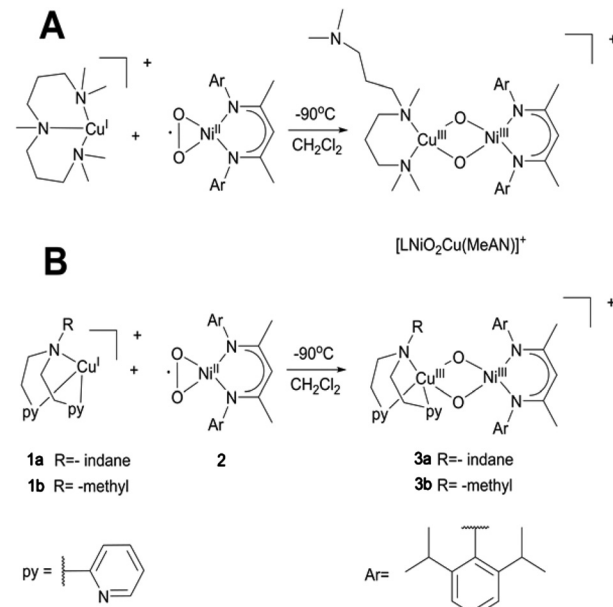


Fig. 1 Two main strategies for the development of heterobimetallic metal-dioxygen complexes.

well-defined dioxygen metal subunit L_nM-O_2 with a low-valent metal complex fragment L'_mM' . This last strategy has been successfully used to generate heterobimetallic oxygen-containing species with $PdMo$,¹⁰ $CuNi$,¹¹ $CuGe$,¹² $PtCu$ ¹³ and $CuPd$ ¹³ combinations, starting from well-defined metal-dioxygen precursors. Our contribution in the field involves the synthesis of a novel family of NiO_2M complexes generated by using a mono-nuclear *side-on* LNi^{II} superoxo precursor bearing a β -diketiminato (Nacnac) ligand ($L = [HC-(CMeNC_6H_3(iPr)_2)_2]$) system.¹⁴ Notably, this precursor is remarkably stable and can be handled at room temperature, which made it a suitable precursor for the synthesis of heterobimetallic metal-dioxygen complexes. Interestingly, in our previous studies, the electronic structure of the $[NiO_2M]^{n+}$ core in such complexes was found to be dependent on the nature of the second metal ion, M ; whereas a peroxido species¹⁵ $[Ni(\mu-O_2)K]^{n+}$ was stabilized in the presence of potassium, replacement of the monovalent potassium ion by LZn^{+} ¹⁵ ($L = \text{Nacnac}$) or LFe^{+} ¹⁶ ions initiated peroxido O–O bond scission and subsequent H-atom abstraction to generate the heterobimetallic bis(μ -hydroxo) $Ni-Zn$ or alkoxo hydroxido $Ni-Fe$ species, respectively. Although the fleeting $[LNiO_2ML]$ ($M = Fe, Zn$) could not be isolated, in a subsequent study a related $[LNiO_2Cu(\text{MeAN})]^{n+}$ species was stabilized at low temperature by reacting the $[LNi^{II}O_2]$ precursor with a copper triamine $[\text{Cu}(\text{MeAN})]^{n+}$ reductant (Scheme 1A). Interestingly, the presence of Cu in the second metal binding site was shown to result in nucleophilic oxo groups in the high-valent bis- μ -oxido $Ni-Cu$ species, and it was able to react towards aldehyde substrates, in contrast to the reported electrophilic properties of the homobimetallic NiO_2Ni , CuO_2Cu and heterobimetallic NiO_2Fe counterparts.¹⁷ In the present manuscript we now try to systematically explore how the nature of the ancillary ligand can modulate the formation, structure, electronic properties and reactivity of such high-valent heterobimetallic dioxygen species. For this purpose, we report on the synthesis, spectroscopy, DFT derived description, and reactivity studies of two new bis- μ -oxido $CuNi$ intermediates, where the triamine MeAN ligand at Cu is replaced by relatively weaker bases/nucleophiles in the bis 2-pyridyl(ethylamine) (RPY_2 ; $R = \text{methyl or indane}$) ligand systems. Notably, the RPY_2 -type ligands have been previously utilised in the formation of binuclear Cu_2^{II} -peroxido complexes, which were shown to exist in equilibrium with the isomeric $Cu_2^{III}(\mu\text{-oxido})$ species depending on the reaction con-



Scheme 1 A: Generation of the $[LNi^{III}O_2Cu^{III}(\text{MeAN})]^{+}$ complex which is already reported.¹⁷ B: Generation of $[LNi^{III}O_2Cu^{III}(\text{RPY}_2)]^{+}$ species **3a** (**3b**) upon mixing a solution of the LNi^{II} superoxo complex **2** with the $(\text{RPY}_2)\text{Cu}^I$ complexes **1a** (or **1b**).

ditions.^{1a} The side-on peroxido dicopper(II) intermediates exhibited electrophilic character towards C–H bond oxygenation of substrates.^{1f,h,i} For example, on using an “indane” substrate covalently attached to the ligand (IndanePY₂, Scheme 1), intramolecular oxygen atom transfer was shown to take place in a highly regio- and stereo-selective manner leading to the *cis*-hydroxylated diastereoisomers of the ligand.¹⁸ The successful generation of the $[LNiO_2\text{Cu}(\text{RPY}_2)]^{+}$ complexes now offers the opportunity to compare and contrast the reactivity of the present complexes with that of the previously reported heterodinuclear $[LNiO_2\text{Cu}(\text{MeAN})]^{+}$ and homodinuclear $\{[\text{Cu}(\text{RPY}_2)]_2\text{O}_2\}^{2+}$ complexes.

Results and discussion

Synthesis and UV-Vis spectroscopy

The complexes **1a** and **1b** were prepared by mixing one molar eq. of $\text{Cu}^I(\text{CH}_3\text{CN})_4(\text{OTf})$ with one molar eq. of ligand in dichloromethane. Equimolar amounts of **1a** $\{(\text{IndanePY}_2)\text{Cu}^I(\text{OTf})\}$ or **1b** $\{(\text{CH}_3\text{PY}_2)\text{Cu}^I(\text{OTf})\}$ and **2** were then mixed at -90°C in dry dichloromethane leading to the immediate formation of the brownish intermediates **3a** $\{[\text{IndanePY}_2]\text{Cu}(\text{O}_2)\text{Ni}[\text{C}-(\text{CMeNC}_6\text{H}_3(i\text{Pr})_2)_2](\text{OTf})\}$ and **3b** $\{[\text{CH}_3\text{PY}_2]\text{Cu}(\text{O}_2)\text{Ni}[\text{C}-(\text{CMeNC}_6\text{H}_3(i\text{Pr})_2)_2](\text{OTf})\}$, respectively (Scheme 1B). The generation of these species was monitored by UV-Vis spectroscopy following the appearance of a characteristic absorption band centred at 885 nm for **3a** and 870 nm for **3b** (Fig. 2). The intermediates are stable at -90°C , but they are thermally sensitive, as indicated by bleaching of their UV-Vis absorption features

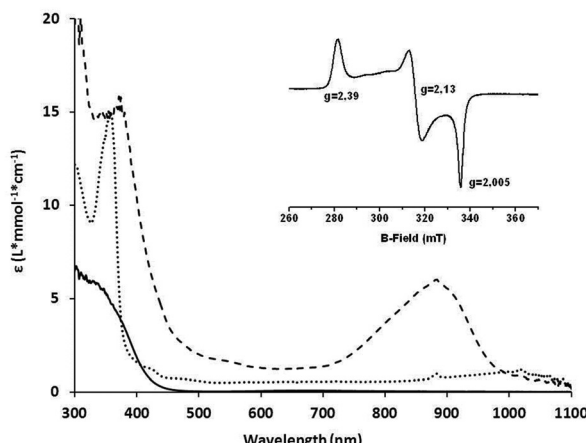


Fig. 2 Absorption spectra of the Cu^I complex (solid trace) **1a**, Ni^{II} superoxo complex **2** (dotted trace) and the 0.15 mM [Ni^{III}(μ -O₂)Cu^{III}]⁺ species **3a** (dashed trace) in dichloromethane at -90 °C. Inset: X-band EPR spectrum of **3a** in dichloromethane at 77 K.

upon warming to higher temperatures (see the ESI†) with $t_{1/2} = 2000$ s at -60 °C.

EPR spectroscopy

The EPR spectra were recorded in frozen CH₂Cl₂ solutions (77 K) for **3a** and **3b** and are very similar for both complexes. The EPR spectrum obtained in the case of **3a** is presented in Fig. 2. The spectra are composed of typical $S = 1/2$ rhombic signals with $g_1 = 2.39$, $g_2 = 2.13$, and $g_3 = 2.005$ for **3a** and $g_1 = 2.39$, $g_2 = 2.13$, and $g_3 = 2.006$ for **3b**. These EPR signals are very similar to the one reported previously for the [LNiO₂Cu(MeAN)]⁺ complex.¹⁷ Notably, no interaction of the electron spin with the nuclear spin of copper is observed for both **3a**/**3b**, consistent with their Ni^{III}(μ -O)₂Cu^{III} assignment, in agreement with the data previously reported in the literature for the Cu-Ni analog.¹⁷

Resonance Raman spectroscopy

The resonance Raman (rRaman) spectra of **3a** and **3b** were recorded using 413 nm laser excitation. rRaman bands are detected at 605 cm⁻¹ and 612 cm⁻¹ for **3a** and **3b**, respectively (Fig. 3, ESI†), which are sensitive to ¹⁸O substitution (performed by using Ni¹⁸O₂ as a starting reagent) and downshift ($\Delta^{18}\text{O}$) by 31 cm⁻¹ and 29 cm⁻¹, respectively. Notably, these bands are shifted to lower energies relative to the tetra-atomic vibrational mode of the [LNi(μ -O₂)Cu(MeAN)]⁺ complex observed at 625 cm⁻¹.¹⁷ Furthermore, as previously observed, the absence of any isotope sensitive bands in the 700–1200 cm⁻¹ region excludes the possibility of the presence of peroxy or superoxo units in **3a** or **3b**. Interestingly, a second ¹⁸O sensitive band is also detected at 556 cm⁻¹ ($\Delta^{18}\text{O} = -21$ cm⁻¹) and 579 cm⁻¹ ($\Delta^{18}\text{O} = -19$ cm⁻¹) for **3a** and **3b** respectively, which was not observed in the previously reported spectrum of the [LNiO₂Cu(MeAN)]⁺ complex.

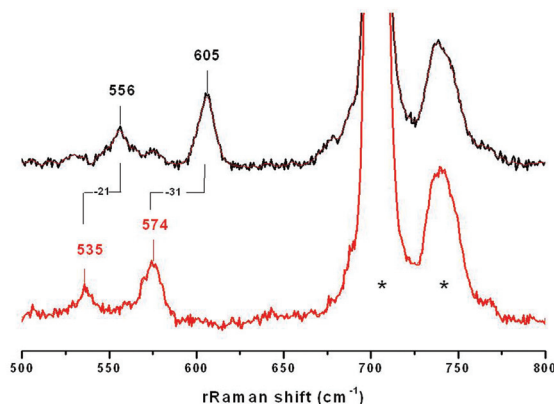


Fig. 3 Raman shifts obtained using a 413 excitation laser for **3a** involving ¹⁶O (top) and ¹⁸O (bottom) atoms. Bands originated from the solvent are marked by asterisks.

DFT calculations

DFT calculations were performed on **3a** and **3b** in an effort to understand their structural and electronic properties as well as the origin of the additional ¹⁸O sensitive band in the rRaman spectra. DFT-optimised structures revealed a four-coordinate distorted square-planar geometry around the nickel centre. Two conformations around the copper ion were computed for each system (conformers A and B). In all cases, the copper site is in a five-coordinate square pyramidal geometry but with either the amine group (conformer A) or one pyridine group (conformer B) weakly bonded to the metal ion in the axial position. Energetic analysis conducted on both **3a** and **3b** showed that the minimum free energy is obtained for the conformers (A) which make these structures the most favoured one (see Table S3; ESI†). The computed structures for **3a** and **3b** (conformers A and B) are presented in Fig. 4, S11 and S12.†

Both spin density plots and Singly Occupied Molecular Orbitals (SOMO) reveal that **3a** and **3b** bear one unpaired electron located at the nickel centre (see Fig. S13 and S14; ESI†). These results confirm the presence of one low-spin Ni^{III} centre ($S = 1/2$, 3d⁷) and one low-spin Cu^{III} ($S = 0$, 3d⁸) centre in both **3a** and **3b**. This assignment is further confirmed by the computed EPR parameters, which are in fair agreement with the experimental data (see Table S4; ESI†). Frequency calculations were conducted on the DFT-optimised structures of the two species and Raman spectra were calculated. Vibration modes involving the oxygen ligands were predicted at 596 cm⁻¹ and 621 cm⁻¹ for **3a** and **3b** (Fig. S15 and S16; Table S5†), respectively, in agreement with the assignment previously proposed for the MeAN-based Cu-Ni analog.¹⁷ A second mode was calculated to be at 553 cm⁻¹ and 528 cm⁻¹ for **3a** and **3b**, respectively, originating from the coupling of the Ni(μ -O₂)Cu core and the Ni-coordinated β -diketiminate ligand coordinates (see Fig. S17 and S18; ESI†). Both sets of the calculated results are in good agreement with the observed rRaman bands for each complex (Table S5; ESI†). The five-coordination geometry at the Cu ions obtained in the case of RPY₂-type ligands is

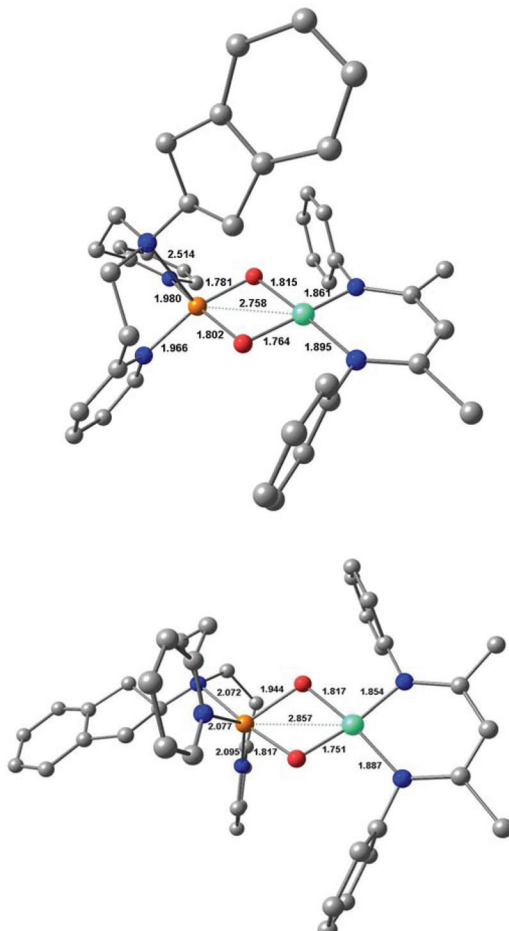


Fig. 4 Optimised molecular structures for **3a**; conformers A (top) and B (bottom).

affecting the coordination sphere of the Ni ion in **3a** and **3b** and the geometry around the Ni ion appears to be significantly distorted from planarity (dihedral angle of 11.2 and 16.2°, respectively) while it is perfectly planar in the MeAN-based complex (dihedral angle of 2.3°). This explains the appearance of a new vibration in the rR spectra of **3a/3b**. The spectroscopic data thus support the DFT-calculated structure and validate the formation of both **3a** and **3b**.

Reactivity studies

The reactivity of the complexes **3a** and **3b** has been investigated in a number of nucleophilic and electrophilic reactions. The nucleophilicity of **3a** and **3b** has been studied in reactions with benzaldehyde, and cyclohexane carboxaldehyde (CCA). The ability of **3a** (**3b**) to undergo electrophilic Hydrogen Atom Transfer (HAT) reactions was also evaluated in reactions with 9,10-dihydroanthracene (DHA) and 1,3-cyclohexadiene (CHD) for C–H bonds and with 2,4-di-*tert*-butylphenol (2,4-DTBP) and 2,6-di-*tert*-butylphenol (2,6-DTBP) for O–H bonds. In a typical reaction preformed **3a** and **3b** at –60 °C were treated with an

excess of the above-mentioned substrates under a pseudo first-order condition.

The disappearance of the characteristic band at 885 nm in the UV-Vis absorption spectrum was then monitored over time (Fig. 5 for reaction of **3a** with CCA). Rate constants in CH_2Cl_2 at –60 °C or at –90 °C were obtained from the pseudo-first order fit of the time trace of the decay of the 885 nm band (Fig. 5). Second-order rate constants were then determined from the dependence of the first-order rate constants on the substrate concentration (Fig. 6). Second-order rate constants derived from those studies are listed in Table 1 and compared with that of the results obtained for the previously reported $[\text{LNiO}_2\text{Cu}(\text{MeAN})]^+$ intermediate. Notably, complex **3b** reacts with CCA and benzaldehyde at rates significantly slower than $[\text{LNiO}_2\text{Cu}(\text{MeAN})]^+$.

In contrast, in the presence of DHA, CHD, 2,4-DTBP, or 2,6-DTBP, complex **3b** is found to be a better oxidant than $[\text{LNiO}_2\text{Cu}(\text{MeAN})]^+$. These studies point to the presence of less nucleophilic oxygen atoms in **3b** relative to $[\text{LNiO}_2\text{Cu}(\text{MeAN})]^+$. Notably, replacement of the methyl group of the MePy₂ ligand in **3b** with a bulkier indane group in **3a** did not lead to any significant change in the rate constants for the reactions with

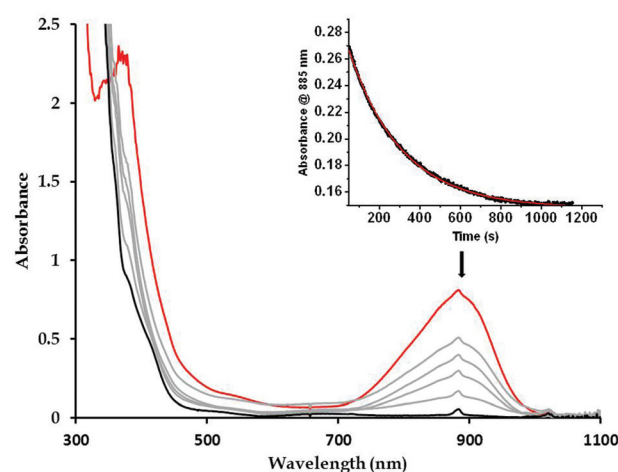


Fig. 5 Spectral changes of **3a** in the presence of 50 mM CCA at –60 °C. Inset: Time trace of the decay at 885 nm band upon addition of the substrate (black trace) and the first-order fit (inset: red trace).

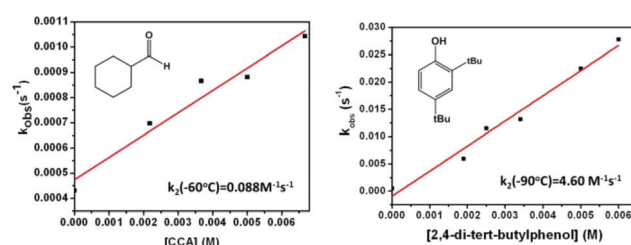


Fig. 6 Pseudo first-order rate constants as a function of substrate concentration; the reaction of **3a** with cyclohexane carboxaldehyde (left) and 2,4-di-*tert*-butylphenol (right) in CH_2Cl_2 .

Table 1 Second order rate constants determined for different substrates by kinetic studies by UV-Vis spectroscopy

Substrates	Benzaldehyde (-60 °C)	CCA (-60 °C)	DHA (-60 °C)	CHD (-60 °C)	2,4 DTBP (-90 °C)	2,6 DTBP (-60 °C)
3a $k_2/M^{-1} s^{-1}$	0.021	0.088	0.015	0.053	4.60	0.0065
3b $k_2/M^{-1} s^{-1}$	0.0178	0.557	0.015	0.014	Too fast	0.0985
$[\text{LNi}^{\text{III}}(\mu\text{-oxo})\text{Cu}^{\text{III}}(\text{MeAN})]^+$	0.11 (-50 °C)	Too fast (-90 °C)	Too slow (-70 °C)	0.0005 (-70 °C)	2.44 (-90 °C)	0.0001 (-80 °C)
$k_2/M^{-1} s^{-1}$						

DHA and benzaldehyde. However, for reactions with bulkier substrates like 2,6-DTBP, 2,4-DTBP, or CCA, a significantly reduced rate constant is observed for **3a** relative to **3b**. This may be attributed to the sterically induced hindered access of the substrates in the presence of the covalently attached indane group of the IndanePY₂ ligand in **3a**. Analysis of the resultant solution after reactions of **3a** or **3b** with various substrates showed the formation of the oxidised products in 45–70% yields (Table S1; ESI†). Interestingly, for reactions with **3a** no evidence of the hydroxylation of the indane moiety was observed, which is in contrast to the previous report of the intramolecular indane hydroxylation reaction mediated by the homodinuclear copper–oxygen intermediate.¹⁸

Additional DFT calculations were performed in order to further characterise the reactivity differences. Natural population analysis was performed for **3a/3b** and the results were compared with those obtained for $[\text{LNi}^{\text{III}}\text{O}_2\text{Cu}^{\text{III}}(\text{MeAN})]^+$ (see the ESI†). The natural negative charges found at the O atoms are smaller (by -7% to -8%) in **3a** and **3b** with respect to those of the corresponding atoms in $[\text{LNi}^{\text{III}}\text{O}_2\text{Cu}^{\text{III}}(\text{MeAN})]^+$. These data indicate that the oxido cores in **3a** and **3b** are less electron-rich compared to that of $[\text{LNi}^{\text{III}}\text{O}_2\text{Cu}^{\text{III}}(\text{MeAN})]^+$. It thus correlates with the decreased nucleophilicity presently observed.

Conclusions

Examples of heterobimetallic dioxygen intermediates are extremely rare in the literature and hence, very little is known about their reactivity. This is unfortunate, as metal dioxygen cores involving non-equivalent metal-sites have been proposed as the active species in a number of biological and chemical oxidation processes, and a detailed knowledge about their reactivity can provide vital mechanistic insights. In our continuous effort to uncover structure–reactivity relationships of unprecedented dinuclear metal–dioxygen intermediates we now investigate the role of ancillary ligands in controlling the spectroscopic and reactivity properties of a heterobimetallic $[\text{Ni}(\mu\text{-O})_2\text{Cu}]^+$ core. The first (and only example before this study of such a core) has been spectroscopically identified in our groups and previously shown to possess a nucleophilic oxo group that led to the deformylation of aldehydes. We now show that the nucleophilicity of the oxo groups can be tuned by varying the electron donation of the ancillary ligand at the copper centre. Thus replacement of the MeAN ligand in the

previously reported $[\text{LNi}(\mu\text{-O}_2)\text{Cu}(\text{MeAN})]^+$ complex by less basic/nucleophilic RPY₂ ligands in **3a/3b** led to slower nucleophilic and faster electrophilic reactions in the latter. Based on the DFT calculations, the difference in reactivity has been attributed to the presence of a five coordinate copper centre and a significant distortion of the nickel centre from planarity in **3a/3b**. These result in the development of lower negative charges at the oxygen atoms of **3a/3b** relative to the $[\text{LNi}(\mu\text{-O}_2)\text{Cu}(\text{MeAN})]^+$ complex, where a four coordinate square planar structure has been reported to be prevalent at both the Cu and Ni centres. Furthermore, for reactions with **3a** no hydroxylation of the indane moiety occurred, in contrast to the previous report of the intramolecular indane hydroxylation reaction mediated by the homodinuclear $\{(indane-py)_2\text{CuO}_2\text{Cu}(indane-py)_2\}$ complex. This again emphasizes the initiation of novel reactivity properties in heterobimetallic systems relative to their homobimetallic counterparts. The present results therefore underline the significance of subtle geometric and electronic changes in the physical and chemical properties of this important class of biologically relevant metal–dioxygen intermediates.

Experimental

All chemicals used in this study except for the ligands and the complexes were commercial products of the highest available purity. Commercial starting materials were used without further purification, except for 2-vinylpyridine which was distilled prior to use. Preparation and handling of air sensitive materials were performed in a N₂ glove box OMNI-Lab 2 (VAC) with O₂ and moisture concentrations less than 2 ppm. ¹H NMR spectra were recorded on a Bruker Avance III 300 MHz NMR spectrometer. UV-Vis spectra were recorded by using an Agilent 8453 diode array spectrophotometer from 300–1100 nm with samples in a 1.0 path length quartz cuvette, connected with a cryostat from Unisoku Scientific Instruments, Japan.

Synthetic procedures

General procedure of synthesis of ligands

CH₃PY₂. The ligand has been synthesized in a slightly different way from the already reported procedure.^{1g} To absolute MeOH (80 mL) were added 2-vinylpyridine (11 g, 0.210 mol), 2-(2-methylaminoethyl) pyridine (4.2 g, 0.030 mol), and glacial acetic acid (1.8 g, 0.060 mol). After refluxing for 5 days under argon, MeOH was evaporated and 15% NaOH was



added. The product was extracted with CH_2Cl_2 ($\times 3$) and the combined organic layers were dried over Na_2SO_4 . Evaporation of CH_2Cl_2 under reduced pressure left the crude product. Flash chromatography (neutral alumina, ethylacetate/MeOH, 98 : 2) afforded the ligand as a yellow product (yield: 40%).

IndanePY₂. The ligand has been synthesized according to the already reported procedure.^{18a}

General procedure of the synthesis of complexes

The complexes **1a** and **1b** have been synthesized *in situ* by the dropwise addition of a solution of 1 eq. $\text{Cu}^{\text{I}}(\text{CH}_3\text{CN})_4\text{OTf}$ in anhydrous dichloromethane in a solution of 1 eq. dissolved ligand in the same solvent.

General procedure for the synthesis of $[\text{LNi}^{\text{III}}(\text{O}_2)\text{Cu}^{\text{III}}(\text{RPy}2)]$

The greenish solution of **2** in anhydrous CH_2Cl_2 (2.5 mL; 0.15 mM) was cooled to $-90\text{ }^{\circ}\text{C}$. Then 1 equivalent of **1a** (**1b**) in anhydrous CH_2Cl_2 (0.1 mL) was added to yield the deep brown intermediate **3a** (**3b**). The generation of the deep brown species **3a** (**3b**) was monitored by the growth of the 885 nm band in the UV-vis spectrum. ¹⁸O labelled samples for rRaman experiments were prepared using the same procedure but starting from ¹⁸O labelled Ni precursor **2**.

EPR spectroscopy

EPR measurements were performed on a Bruker ESP 300 X-band EPR spectrometer equipped with a fused quartz Dewar for measurements at liquid nitrogen temperature.

Resonance Raman

rRaman spectra were recorded in CH_2Cl_2 at $-92\text{ }^{\circ}\text{C}$ (Bruker cryostat) using 413 nm excitation with a Horiba Jobin-Yvon LabRAM HR800 confocal Raman spectrometer. The concentrations of samples were from 3 mM to 8 mM.

DFT calculations

All theoretical calculations were performed with the ORCA program package.¹⁹ Full geometry optimizations were carried out for all complexes using the GGA functional BP86^{20–22} in combination with the TZV/P²³ basis set for all atoms and by taking advantage of the resolution of the identity (RI) approximation in the Split-RI-J variant²⁴ with the appropriate Coulomb fitting sets.²⁵ Increased integration grids (Grid4 in ORCA convention) and tight SCF convergence criteria were used. Solvent effects were accounted within the framework of the conductor like screening model (COSMO) which is a dielectric continuum approach.²⁶ Vibrational frequency calculations were performed to ensure that each geometry optimization converged to a real minimum. IR and rRaman spectra were obtained from numerical frequency calculations performed on the optimised structures using the B3LYP^{27,28} functional together with the TZV/P²³ basis set. The relative energies were obtained from single-point calculations using the same combination of functional and basis sets. They were computed from the gas-phase optimised structures as a sum of electronic energy, thermal corrections to free energy, and free energy of

solvation. *g*-Tensors^{29–32} were evaluated from additional single point calculations using the B3LYP functional. Scalar relativistic effects were included with ZORA paired using the SARC def2-TZVP(-f) basis sets^{33,34} and the decontracted def2-TZVP/J Coulomb fitting basis sets for all atoms. Increased integration grids (Grid4 and GridX4 in ORCA convention) and tight SCF convergence criteria were used. Picture change effects were applied and the integration grids were increased to an integration accuracy of 11 (ORCA convention) for the metal centre. Natural charges were obtained from additional single-point calculations using the Natural Population Analysis (NPA) and the B3LYP functional together with the TZV/P basis set.³⁵ Molecular orbitals, spin density plots and vibrational normal modes were visualized with Chemcraft software.³⁶

Reactivity studies

Exogenous substrate oxidation. In a typical experiment, 0.15 mM to 0.2 mM of **3a** (**3b**) was generated at $-90\text{ }^{\circ}\text{C}$, as discussed previously. The reactivity studies of **3a** (**3b**) were performed at $-60\text{ }^{\circ}\text{C}$ under an inert atmosphere, by injecting the CH_2Cl_2 solution of the substrate (varying from 1 mM to 60 mM). Spectral changes at the 885 nm band were monitored by using a UV-Vis spectrum every 1 second. The pseudo-first order oxidation rate was then extracted and compared with the self decay of **3a** (**3b**) in the absence of the substrate. If the rate of oxidation in the presence of the substrate was higher than that in the absence of the substrate, it was concluded that **3a** (**3b**) reacted with that substrate. The pseudo-first order fitting of the decay curves yielded the rate constants (k_{obs}), which follow linear dependence with the concentration of the substrate. The slope of the rate constant (k_{obs}) *versus* substrate concentration fitting plot provided the second order rate constants (k_2).

Intramolecular ligand oxidation. The brownish solution of **3a** was warmed up at room temperature. The solution was treated with 35% ammonia solution and after extraction with dichloromethane ($\times 2$) the organic phases were washed with brine ($\times 2$); the organic phases were collected, dried over MgSO_4 and the solvent was removed under vacuum. The resulting solid was analysed by ¹H NMR spectroscopy and mass spectrometry which showed the absence of the hydroxylated product.

Acknowledgements

This work has been carried out in the framework of COST action CM1305 (ECOSTBio) including two STSMs (STSM-CM1305-28897 and STSM-CM1305-32182). Financial support by the French Research Agency (COMEBAC/ANR-13-BS07-0018) as well as from the DFG (Cluster of Excellence “Unifying Concepts in Catalysis”; EXC 314-2) is gratefully acknowledged. K. R. also thanks the Heisenberg-Program of DFG for financial support.



Notes and references

1 (a) L. M. Mirica, X. Ottenwaelder and T. D. P. Stack, *Chem. Rev.*, 2004, **104**, 1013–1046; (b) E. A. Lewis and W. B. Tolman, *Chem. Rev.*, 2004, **104**, 1047–1076; (c) T. Osako, S. Terada, T. Toshia, S. Nagatomo, H. Furutachi, S. Fujinami, T. Kitagawa, M. Suzuki and S. Itoh, *Dalton Trans.*, 2005, 3514–3521; (d) L. Hatcher and K. D. Karlin, *J. Biol. Inorg. Chem.*, 2004, **9**, 669–683; (e) M. Schatz, M. Becker, F. Thaler, F. Hampel, S. Schindler, R. R. Jacobson, Z. Tyeklár, N. N. Murthy, P. Ghosh, Q. Chen, J. Zubietta and K. D. Karlin, *Inorg. Chem.*, 2001, **40**, 2312–2322; (f) H. V. Obias, Y. Lin, N. N. Murthy, E. Pidcock, E. I. Solomon, M. Ralle, N. J. Blackburn, Y.-M. Neuhold, A. D. Zuberbühler and K. D. Karlin, *J. Am. Chem. Soc.*, 1998, **120**, 12960–12961; (g) I. Sanyal, M. Mahroof-Tahir, M. S. Nasir, P. Ghosh, B. I. Cohen, Y. Gultneh, R. W. Cruse, A. Farooq and K. D. Karlin, *Inorg. Chem.*, 1992, **31**, 4322–4332; (h) C. Xin Zhang, H.-C. Liang, E.-i. Kim, J. Shearer, M. E. Helton, E. Kim, S. Kaderli, C. D. Incarvito, A. D. Zuberbühler, A. L. Rheingold and K. D. Karlin, *J. Am. Chem. Soc.*, 2003, **125**, 634–635; (i) J. Shearer, C. Xin Zhang, L. N. Zakharov, A. L. Rheingold and K. D. Karlin, *J. Am. Chem. Soc.*, 2005, **127**, 5469–5483.

2 (a) R. Manchanda, G. W. Brudvig and R. H. Crabtree, *Coord. Chem. Rev.*, 1995, **144**, 1–38; (b) A. J. Wu, J. E. Penner-Hahn and V. L. Pecoraro, *Chem. Rev.*, 2004, **104**, 903–938.

3 (a) R. Schenker, B. S. Mandimutsira, C. G. Riordan and T. C. Brunold, *J. Am. Chem. Soc.*, 2002, **124**, 13842–13855; (b) K. Shiren, S. Ogo, S. Fujinami, H. Hayashi, M. Suzuki, A. Uehara, Y. Watanabe and Y. Moro-oka, *J. Am. Chem. Soc.*, 2000, **122**, 254–262; (c) S. Itoh, H. Bandoh, M. Nakagawa, S. Nagatomo, T. Kitagawa, K. D. Karlin and S. Fukuzumi, *J. Am. Chem. Soc.*, 2001, **123**, 11168–11178.

4 (a) S. Hikichi, M. Yoshizawa, Y. Sasakura, M. Akita and Y. Moro-oka, *J. Am. Chem. Soc.*, 1998, **120**, 10567–10568; (b) S. Hikichi, M. Yoshizawa, Y. Sasakura, H. Komatsuzaki, Y. Moro-oka and M. Akita, *Chem. – Eur. J.*, 2001, **7**, 5011–5028.

5 A. J. Skulan, M. A. Hanson, H. Hsu, L. Que Jr. and E. I. Solomon, *J. Am. Chem. Soc.*, 2003, **125**, 7344–7356.

6 (a) P. R. Sharp, *J. Chem. Soc., Dalton Trans.*, 2000, 2647–2657; (b) J. J. Li, W. Li and P. R. Sharp, *Inorg. Chem.*, 1996, **35**, 604–613.

7 H. Decker, R. Dillinger and F. Tuczek, *Angew. Chem., Int. Ed.*, 2000, **39**, 1591–1595.

8 R. L. Lieberman and A. C. Rosenzweig, *Dalton Trans.*, 2005, 3390–3396.

9 I. Garcia-Bosch, X. Ribas and M. Costas, *Eur. J. Inorg. Chem.*, 2012, 179–187.

10 P. L. Alsters, J. Boersma and G. van Koten, *Organometallics*, 1993, **12**, 1629–1638.

11 N. W. Aboeella, J. T. York, A. M. Reynolds, K. Fujita, C. R. Kinsinger, C. J. Cramer, C. G. Riordan and W. B. Tolman, *Chem. Commun.*, 2004, 1716–1717.

12 J. T. York, V. G. Young Jr. and W. B. Tolman, *Inorg. Chem.*, 2006, **45**, 4191–4198.

13 J. T. York, A. Llobet, C. J. Cramer and W. B. Tolman, *J. Am. Chem. Soc.*, 2007, **129**, 7990–7999.

14 S. Yao, E. Bill, C. Milsmann, K. Wieghardt and M. Driess, *Angew. Chem., Int. Ed.*, 2008, **47**, 7110–7113.

15 S. Yao, Y. Xiong, M. Vogt, H. Grützmacher, C. Herwig, M. C. Limberg and M. Driess, *Angew. Chem., Int. Ed.*, 2009, **48**, 8107–8110.

16 S. Yao, C. Herwig, Y. Xiong, A. Company, E. Bill, C. Limberg and M. Driess, *Angew. Chem., Int. Ed.*, 2010, **39**, 7208–7212.

17 S. Kundu, F. F. Pfaff, E. Miceli, I. Zaharieva, C. Herwig, S. Yao, E. R. Farquhar, U. Kuhlmann, E. Bill, P. Hildebrandt, H. Dau, M. Driess, C. Limberg and K. Ray, *Angew. Chem., Int. Ed.*, 2013, **52**, 5622–5626.

18 (a) I. Blain, P. Bruno, M. Giorgi, E. Lojou, D. Lexa and M. Réglier, *Eur. J. Inorg. Chem.*, 1998, 1297–1304; (b) I. Blain, M. Giorgi, I. De Riggis and M. Réglier, *Eur. J. Inorg. Chem.*, 2000, 393–398; (c) I. Blain, M. Giorgi, I. De Riggis and M. Réglier, *Eur. J. Inorg. Chem.*, 2001, 205–211.

19 F. Neese, *Wiley Interdiscip. Rev.: Comput. Mol. Sci.*, 2012, **2**, 73–78.

20 J. P. Perdew, *Phys. Rev. B: Condens. Matter*, 1986, **33**, 8822.

21 J. P. Perdew, *Phys. Rev. B: Condens. Matter*, 1986, **34**, 7406.

22 A. D. Becke, *Phys. Rev. A*, 1988, **38**, 3098–3100.

23 A. Schäfer, C. Huber and R. J. Ahlrichs, *J. Chem. Phys.*, 1994, **100**, 5829–5835.

24 F. Neese, *J. Comput. Chem.*, 2003, **24**, 1740–1747.

25 F. Weigend, *Phys. Chem. Chem. Phys.*, 2006, **8**, 1057–1065.

26 A. Klamt and G. Schüürmann, *J. Chem. Soc., Perkin Trans. 2*, 1993, 799–805.

27 A. D. Becke, *J. Chem. Phys.*, 1993, **98**, 1372.

28 C. T. Lee, W. T. Yang and R. G. Parr, *Phys. Rev. B: Condens. Matter*, 1988, **37**, 785–789.

29 F. Neese, *J. Chem. Phys.*, 2001, **115**, 11080–11096.

30 S. Koseki, M. W. Schmidt and M. S. Gordon, *J. Chem. Phys.*, 1992, **96**, 10768–10772.

31 S. Koseki, M. S. Gordon, M. W. Schmidt and N. J. Matsunaga, *J. Chem. Phys.*, 1995, **99**, 12764–12772.

32 F. Neese, *J. Chem. Phys.*, 2003, **118**, 3939.

33 D. A. Pantazis, X.-Y. Chen, C. R. Landis and F. Neese, *J. Chem. Theory Comput.*, 2008, **4**, 908–919.

34 D. A. Pantazis and F. Neese, *J. Chem. Theory Comput.*, 2009, **5**, 2229–2238.

35 A. E. Reed, R. B. Weinstock and F. Weinhold, *J. Chem. Phys.*, 1985, **83**, 735–746.

36 Chemcraft, <http://chemcraftprog.com>.

